International Journal of Solids and Structures 50 (2013) 4118–4132

Contents lists available at ScienceDirect

International Journal of Solids and Structures

journal homepage: www.elsevier.com/locate/ijsolstr

An improved model of thin cylindrical piezoelectric layers between isotropic elastic media

S. Abdel-Gawad, Xiaodong Wang *

Department of Mechanical Engineering, University of Alberta, Edmonton, AB T6G 2G8, Canada

ARTICLE INFO

Article history:
Received 16 May 2013
Received in revised form 8 August 2013
Available online 27 August 2013

Keywords:
Interphase
Cylindrical
Anisotropy
Composites
Fibres
Dynamic
Piezoelectric

ABSTRACT

Radially polarized piezoelectric fibers are now considered to be used in smart composites. The piezoelectric layers in these fibers are generally anisotropic in the transverse direction and therefore difficult to analyze when dynamic loads are involved. The present paper presents a theoretical study of the dynamic behavior of radially polarized cylindrical piezoelectric layers between isotropic elastic media. A new interphase model is developed to provide simple yet accurate evaluation of the dynamic response of such anisotropic elastic layers. Unlike the traditional interface-spring model, the current interphase model satisfies the equations of motion of the layers and can provide reliable prediction of the stress and displacement. A comparison between the developed model, the interface-spring model and the finite element analysis is conducted. The results clearly show the advantages of the current model over the traditional interface-spring model in simulating anisotropic layers. Numerical examples based on this interphase model for different interphase thicknesses, loading frequencies and material combinations are presented to evaluate the dynamic behavior of multilayered elastic media.

1. Introduction

In addition to the well known advantages of traditional composites, such as higher strength-to-weight ratio and tailored design, smart composites also offer multifunctionality (Gibson, 2010) and, therefore, are receiving significant attention from the research community (Kreja, 2011; Lin and Sodano, 2008). Recent progress in manufacturing multilayered piezoelectric fibers with a transverse poling direction in the cross section makes it possible to develop new smart composites, which can be used in different high frequency applications (Egusa et al., 2010). The fibers have been used to design single-fiber resonators and piezoelectric transducers. It is a natural step to use these fibers to develop smart multifunctional composite materials.

An important issue in the study of this type of smart composites is how to evaluate the piezoelectric layer in the fiber. Since the piezoelectric layer is poled transversely in the cross section and is in general anisotropic, existing solutions for isotropic or transversely-isotropic layers are not sufficient for describing the behavior of the layer. Considering the fact that the piezoelectric layer is relatively thin compared with the radius of the fiber, simplified layer models could be used to overcome this difficulty. Modeling of thin layers in composite materials has been extensively investigated (Kushch et al., 2011; Rajabi and Hasheminejad, 2009; Zhong and Meguid, 1997) because of its importance. In these cases, an interphase, which may represent a bonding layer or an imperfect interface caused by deterioration, is usually modeled by distributed interface springs.

When high frequency dynamic loading is applied, the inertial effect of the anisotropic layer needs to be considered. Solutions for the response of anisotropic materials to general dynamic loads or elastic waves are usually complicated and difficult to obtain, although the corresponding problems for isotropic elastic media can be easily dealt with by determining the displacement potentials based on Helmholtz decomposition (Achenbach et al., 1972). In general cases, the dynamic displacement field in an anisotropic elastic medium can no longer be decomposed into independent displacement potentials. Therefore, well known solution techniques applicable to isotropic media, based on displacement potentials, cannot be applied directly to anisotropic media. The interaction between elastic waves and anisotropic layers in planar layered media has been studied analytically and numerically (Rokhlin and Huang, 1992; Rokhlin and Huang, 1993). The analytical solution is quite complicated, involving the solution of eigenvalue problems. The corresponding problems for cylindrical layers have also been studied under simplified geometric or loading conditions, such as assuming isotropy in the cylinder cross section (Sodagar and Honarvar, 2010; Nayfeh et al., 2000; Nayfeh and Nagy, 1996; Nayfeh et al., 1995; Honarvar and Sinclair, 1996). Numerical solutions for more general anisotropic cylindrically layered media under elastic waves have also been reported in recent

* Corresponding author.
E-mail address: xiaodong.wang@ualberta.ca (X. Wang).

0020-7683/$ - see front matter © 2013 Elsevier Ltd. All rights reserved.
http://dx.doi.org/10.1016/j.ijsolstr.2013.08.026

literatures (Norris and Shuvalov, 2012; Norris and Shuvalov, 2010; Gsell and Dual, 2004). But simplified analytical models for transversely anisotropic cylindrical layers under general dynamic loading are limited to interface-spring models.

For the case of radially poled piezoelectric fibers, the piezoelectric layer poses problems in modeling the mechanical behavior because of both its anisotropy and curvature. A possible method in modeling the layer is to simplify it as distributed interface springs to simulate the traction-displacement relation across the layer. The spring model (Bian et al., 2008; Librescu and Schmidt, 2001; Zhong and Meguid, 1997; Aboudi, 1987) ignores, however, the hoop stress and the inertial effect, and assumes that the stresses are uniform across the thickness of the layer. As a result, the equations of motion of the layer are not satisfied. It should be mentioned that in a typical radially poled piezoelectric fiber (Egusa et al., 2010), the layer thickness could be as large as 20% of the radius of the fiber and the hoop stress in the curved layer may play a significant role in the deformation. It is therefore desirable to develop an interphase model which can represent the effect of the stress variation across the layer thickness, the hoop stress in the layer and the anisotropy of the layer.

The objective of this paper is to develop a new interphase model for anisotropic layers in multilayered cylindrical piezoelectric fibers. Comparison with traditional interface-spring model and finite element analysis indicates that the current model is more accurate than the spring model. Typical simulation results based on the developed model are provided to illustrate the mechanical property of the anisotropic cylindrical layers under dynamic loads.

2. Problem formulation

Consider the cross section of a cylindrical multilayered piezoelectric medium consisting of an inner core $0 < r < r_0$, a piezoelectric layer $r_0 < r < r_1$ and an outer layer $r_1 < r < r_2$, as shown in Fig. 1(a). The inner core and the outer layer are linearly elastic, homogenous and isotropic insulators. These three layers are assumed to be bonded perfectly at the interfaces. Plane strain deformation is considered, which corresponds to the case where the out-of-plane dimension of the medium is significantly greater than its typical radius. The piezoelectric layer is poled along the radial direction and is, therefore, anisotropic in the cross section. The medium is subjected to general mechanical loading along the outer surface. In the limiting case that r_2 approaches infinity, as shown in Fig. 1(b), the load could be an incident wave.

The dynamic load is assumed to be time harmonic and only the steady state response of the medium is considered. The time dependence of the response can be expressed by an exponential function $e^{-i\omega t}$ where t and ω are time and frequency, respectively. For convenience, the term $e^{-i\omega t}$ will be omitted in the following discussion and only the amplitude of the field variables will be considered.

2.1. Governing equations

The dynamic electromechanical property of piezoelectric materials, such as the media shown in Fig. 1, is governed by the equations of motion and Gauss's law (Achenbach et al., 1972; Kessler and Kosloff, 1991). In the polar coordinate system $(r,\ \theta)$ the governing equations are

Equations of Motion

$$\sigma_{r,r} + \frac{1}{r}\sigma_{\theta r,\theta} + \frac{1}{r}(\sigma_r - \sigma_\theta) = -\rho\omega^2 u_r \tag{1}$$

$$\sigma_{r\theta,r} + \frac{1}{r}\sigma_{\theta,\theta} + \frac{2}{r}(\sigma_{r\theta}) = -\rho\omega^2 u_\theta \tag{2}$$

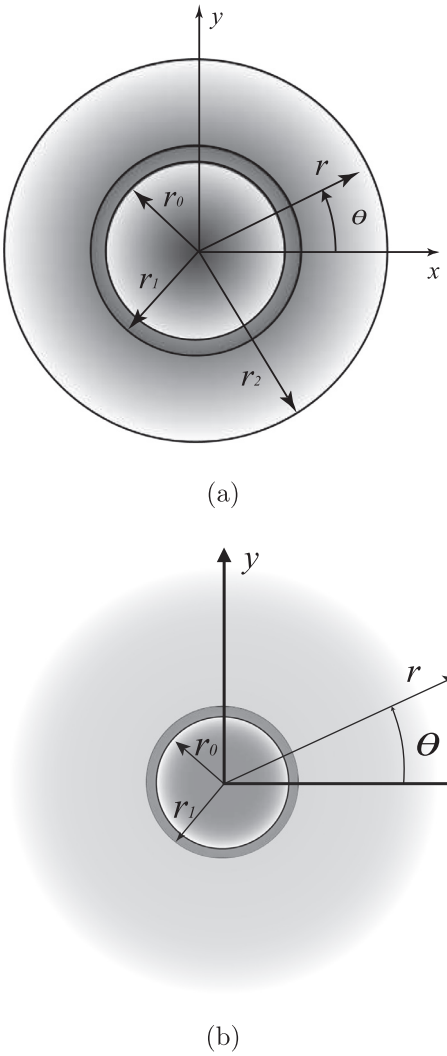

Fig. 1. The layered composite medium with (a) bounded outer layer and (b) unbounded outer medium.

Gauss's Law

$$D_{r,r} + \frac{1}{r}(D_{\theta,\theta} + D_r) = 0 \tag{3}$$

where σ is the stress, u is the displacement, D is the electric displacement and ρ is the density. The subscripts indicate the corresponding components in the polar coordinate system while the comma indicates differentiation, as commonly used. The constitutive relations of the piezoelectric layer, with the poling direction being along r, are given by,

$$\begin{bmatrix}\sigma_r\\ \sigma_\theta\\ \sigma_{\theta r}\end{bmatrix} = \begin{bmatrix}c_{33} & c_{23} & 0\\ c_{23} & c_{22} & 0\\ 0 & 0 & c_{44}\end{bmatrix}\begin{bmatrix}\varepsilon_r\\ \varepsilon_\theta\\ \varepsilon_{r\theta}\end{bmatrix} - \begin{bmatrix}e_{33} & 0\\ e_{32} & 0\\ 0 & e_{24}\end{bmatrix}\begin{bmatrix}E_r\\ E_\theta\end{bmatrix} \tag{4}$$

$$\begin{bmatrix}D_r\\ D_\theta\end{bmatrix} = \begin{bmatrix}e_{33} & e_{32} & 0\\ 0 & 0 & e_{24}\end{bmatrix}\begin{bmatrix}\varepsilon_r\\ \varepsilon_\theta\\ \varepsilon_{r\theta}\end{bmatrix} + \begin{bmatrix}\epsilon_{33} & 0\\ 0 & \epsilon_{22}\end{bmatrix}\begin{bmatrix}E_r\\ E_\theta\end{bmatrix} \tag{5}$$

where c's are the elastic coefficients, ϵ's are the dielectric constants, and e's are the piezoelectric constants, ε represents the strain and E represents the electric field intensity, which can be expressed in terms of the displacements u_r and u_θ, and the electric potential ϕ as

$$\varepsilon_r = u_{r,r} \tag{6}$$

$$\varepsilon_\theta = \frac{1}{r}(u_{\theta,\theta} + u_r) \tag{7}$$

$$\varepsilon_{r\theta} = \frac{1}{2}\left(\frac{1}{r}u_{r,\theta} + u_{\theta,r} - \frac{u_\theta}{r}\right) \tag{8}$$

$$E_r = -\phi_{,r} \tag{9}$$

$$E_\theta = -\frac{1}{r}\phi_{,\theta}. \tag{10}$$

Since the main concern of the current study is how to model the mechanical property of the anisotropic layer under dynamic loads, the outer and inner surfaces of the piezoelectric layer are short circuited so only the mechanical response is included. In this case, E_r= E_θ = 0 and charges at outer and inner surfaces of the piezoelectric layer will be generated but will not affect the stresses.

2.2. Elastic fields in the inner core and the outer medium

The inner core and the outer medium are linearly elastic, homogenous and isotropic. In this case, the displacement field can be decomposed into (Achenbach et al., 1972)

$$u_r = \varphi_{,r} + \frac{1}{r}\psi_{,\theta} \tag{11}$$

$$u_\theta = \frac{1}{r}\varphi_{,\theta} - \psi_{,r} \tag{12}$$

where φ and ψ are two displacement potentials satisfying Helmholtz equation, i.e.

$$\frac{1}{r}(r\varphi_{,r})_{,r} + \frac{1}{r^2}\varphi_{,\theta\theta} + k_L^2\varphi = 0 \tag{13}$$

$$\frac{1}{r}(r\psi_{,r})_{,r} + \frac{1}{r^2}\psi_{,\theta\theta} + k_T^2\psi = 0 \tag{14}$$

k_L and k_T are two wave numbers given by

$$k_L = \frac{\omega}{c_L}, \quad k_T = \frac{\omega}{c_T} \tag{15}$$

where c_L and c_T are the longitudinal and transverse wave speeds of the elastic medium, and

$$c_L = \sqrt{\frac{\lambda + 2\mu}{\rho}}, \quad c_T = \sqrt{\frac{\mu}{\rho}} \tag{16}$$

with λ and μ being the Lame constants of the elastic medium.

The general solutions of the displacement potentials in these layers can be determined by solving Eqs. (13) and (14) using Fourier expansion with respect to θ. The resulting displacement potentials are

$$\varphi(r,\theta) = \sum_{n=0}^{\infty}\left\{J_n(k_L r)\begin{pmatrix}A_n^{(1)}\\A_n^{(2)}\end{pmatrix}^T + H_n^{(1)}(k_L r)\begin{pmatrix}A_n^{(3)}\\A_n^{(4)}\end{pmatrix}^T\right\}\begin{pmatrix}cos(n\theta)\\sin(n\theta)\end{pmatrix} \tag{17}$$

$$\psi(r,\theta) = \sum_{n=0}^{\infty}\left\{J_n(k_T r)\begin{pmatrix}A_n^{(5)}\\A_n^{(6)}\end{pmatrix}^T + H_n^{(1)}(k_T r)\begin{pmatrix}A_n^{(7)}\\A_n^{(8)}\end{pmatrix}^T\right\}\begin{pmatrix}cos(n\theta)\\sin(n\theta)\end{pmatrix} \tag{18}$$

where $J_n(\cdot)$ and $H_n^{(1)}(\cdot)$ are Bessel functions and Hankel functions of the first kind, respectively, and A_n are unknown constants to be determined from the boundary and interface conditions. For the inner core $A_n^{(3)}$, $A_n^{(4)}$, $A_n^{(7)}$, $A_n^{(8)}$ are zero to ensure that the field has a limited amplitude at $r = 0$. If the outer layer is infinite, then $A_n^{(1)}$, $A_n^{(2)}$, $A_n^{(5)}$, $A_n^{(6)}$ will be zero to satisfy the radiation condition at infinity for the scattered wave.

2.3. The interphase model for the anisotropic piezoelectric layer

The piezoelectric layer is transversely anisotropic in the cross section since it is poled in the radial direction. For such an anisotropic medium under dynamic loading, the general analytical solution could not be easily found. In the current subsection, a new interphase model will be presented, which could be used to simulate the dynamic mechanical property of the layer.

The governing equations for the piezoelectric layer, (1) and (2), can be re-written as

$$\frac{1}{r}\left((r\sigma_r)_{,r} + \sigma_{\theta r,\theta} - \sigma_\theta\right) = -\rho\omega^2 u_r \tag{19}$$

$$\frac{1}{r^2}\left((r^2\sigma_{r\theta})_{,r} + r\sigma_{\theta,\theta}\right) = -\rho\omega^2 u_\theta. \tag{20}$$

To overcome the difficulties associated with the anisotropy of the layer, for a relatively thin layer, the derivative with respect to r in these equations is simplified such that $(r\sigma_r)_{,r} \approx \frac{\Delta(r\sigma_r)}{h}$ and $(r^2\sigma_{r\theta})_{,r} \approx \frac{\Delta(r^2\sigma_{r\theta})}{r^2}$ with $h = r_1 - r_0$ being the thickness of the layer and Δ representing the change from r_0 to r_1. Eqs. (19) and (20) can then be approximately expressed as

$$\frac{1}{r}\left(\frac{\Delta(r\sigma_r)}{h} + \sigma_{\theta r,\theta} - \sigma_\theta\right) = -\rho\omega^2 u_r \tag{21}$$

$$\frac{1}{r^2}\left(\frac{\Delta(r^2\sigma_{r\theta})}{h} + r\sigma_{\theta,\theta}\right) = -\rho\omega^2 u_\theta. \tag{22}$$

The layer can now be modeled as a one dimensional element governed by Eqs. (21) and (22). A stress component is decomposed into two parts, (i) a uniform stress across the thickness of the layer element, representing the average stress and (ii) a linear stress across the thickness with a zero average, resulting in the 'Δ' terms in Eqs. (21) and (22), which represent the general 'body forces' acting on the interphase. The other terms in Eqs. (21) and (22), except for the terms with r derivative, are the average values over the thickness of the layer.

The constitutive Eq. (4) can be rewritten in terms of the displacements in the layer as

$$\sigma_r = c_{33}u_{r,r} + \frac{c_{23}}{r}(u_{\theta,\theta} + u_r) \tag{23}$$

$$\sigma_\theta = c_{23}u_{r,r} + \frac{c_{22}}{r}(u_{\theta,\theta} + u_r) \tag{24}$$

$$\sigma_{r\theta} = c_{44}\left(\frac{1}{r}u_{r,\theta} + u_{\theta,r} - \frac{u_\theta}{r}\right). \tag{25}$$

For the layer element the derivatives with respect to r in these equations can be approximated, such that

$$u_{r,r} = \frac{\triangle u_r}{\triangle r}, \quad u_{\theta,r} = \frac{\triangle u_\theta}{\triangle r} \tag{26}$$

and the stress should be considered to be the average value across the thickness.

Substituting Eq. (26) into Eqs. (23)–(25) the constitutive equations for the interphase can be written as

$$\sigma_r = c_{33}\left(\frac{u_r^+ - u_r^-}{h}\right) + \frac{c_{23}}{r}\left(\frac{u_{\theta,\theta}^+ + u_{\theta,\theta}^-}{2} + \frac{u_r^+ + u_r^-}{2}\right) \tag{27}$$

$$\sigma_\theta = c_{23}\left(\frac{u_r^+ - u_r^-}{h}\right) + \frac{c_{22}}{r}\left(\frac{u_{\theta,\theta}^+ + u_{\theta,\theta}^-}{2} + \frac{u_r^+ + u_r^-}{2}\right) \tag{28}$$

$$\sigma_{r\theta} = c_{44}\left(\frac{1}{r}\frac{u^+_{r,\theta}+u^-_{r,\theta}}{2}+\frac{u^+_\theta-u^-_\theta}{h}-\frac{1}{r}\frac{u^+_\theta+u^-_\theta}{2}\right) \tag{29}$$

where the superscripts (+) and (−) refer to the outer and inner surfaces of the layer, and the averaged values in these equations are given by

$$\sigma_r = \frac{\sigma^+_r+\sigma^-_r}{2} \tag{30}$$

$$\sigma_{r\theta} = \frac{\sigma^+_{r\theta}+\sigma^-_{r\theta}}{2} \tag{31}$$

$$r = \frac{r_1+r_0}{2}. \tag{32}$$

Finally, substituting Eqs. (27)–(29) into the equations of motion (21) and (22) results in the following equations for the layer,

$$\frac{1}{r^2}\left\{\frac{r_1^2\sigma^+_{r\theta}-r_0^2\sigma^-_{r\theta}}{h}+r\left[c_{23}\frac{u^+_{r,\theta}-u^-_{r,\theta}}{h}+\frac{c_{22}}{r}\left(\frac{u^+_{\theta,\theta\theta}+u^-_{\theta,\theta\theta}}{2}+\frac{u^+_{r,\theta}+u^-_{r,\theta}}{2}\right)\right]\right\} = -\rho\omega^2\left(\frac{u^+_\theta+u^-_\theta}{2}\right) \tag{33}$$

$$\frac{1}{r}\left\{\frac{r_1\sigma^+_r-r_0\sigma^-_r}{h}+\frac{\sigma^+_{r\theta,\theta}+\sigma^-_{r\theta,\theta}}{2}-\left[c_{23}\frac{u^+_r-u^-_r}{h}+\frac{c_{22}}{r}\left(\frac{u^+_{\theta,\theta}+u^-_{\theta,\theta}}{2}+\frac{u^+_r+u^-_r}{2}\right)\right]\right\} = -\rho\omega^2\left(\frac{u^+_r+u^-_r}{2}\right) \tag{34}$$

and the constitutive relations of the layer become

$$\frac{\sigma^+_r+\sigma^-_r}{2} = c_{33}\frac{u^+_r-u^-_r}{h}+\frac{c_{23}}{r}\left(\frac{u^+_{\theta,\theta}+u^-_{\theta,\theta}}{2}+\frac{u^+_r+u^-_r}{2}\right) \tag{35}$$

$$\frac{\sigma^+_{r\theta}+\sigma^-_{r\theta}}{2} = c_{44}\left(\frac{1}{r}\frac{u^+_{r,\theta}+u^-_{r,\theta}}{2}+\frac{u^+_\theta-u^-_\theta}{h}-\frac{1}{r}\frac{u^+_\theta+u^-_\theta}{2}\right). \tag{36}$$

Eqs. (33)–(36) established a new interphase model, which relates the outer (+) and inner (−) surfaces of the layer based on the property of the layer itself. The model satisfies the equations of motion and the constitutive relations of the layer.

The commonly used interface-spring model can be represented as (Rajabi and Hasheminejad, 2009; Bian et al., 2008),

$$\sigma^+_r = \sigma^-_r = \frac{c_{33}}{h}\left(u^+_r-u^-_r\right) \tag{37}$$

$$\sigma^+_{r\theta} = \sigma^-_{r\theta} = \frac{c_{44}}{h}\left(u^+_\theta-u^-_\theta\right) \tag{38}$$

which assumes a simple linear relation between displacements and stresses across the thickness of the layer. In comparison, in the traditional interface-spring model σ_r and $\sigma_{r\theta}$ are assumed to be constants across the thickness of the layer. σ_θ and the inertial force of the layer are ignored. Only when the thickness of the interphase approaches zero, $h \to 0$, the two models become identical. The spring model is therefore a special case of the currently proposed model.

To determine the solution for a specific boundary condition, the governing Eqs. (33)–(36) for the layer should be combined with the general solutions for the inner core and the outer medium, as given by Eqs. (17) and (18). The continuity condition for stresses and displacements between different layers should be satisfied. Therefore, the components with superscript (+) equal to the values of the corresponding components for the outer medium at $r = r_1$, and the components with superscript (−) equal to that for the inner core at $r = r_0$. The general expressions of the stress and displacement fields can be obtained directly from the displacement potentials given by Eqs. (17) and (18). The results are provided in Appendix A.

By substituting these stress and displacement components into Eqs. (33)–(36), a set of linear equations can be obtained, from which the unknown coefficients $A_n^{(1)}$ to $A_n^{(8)}$ in Eqs. (17) and (18) can be determined for specific boundary conditions.

It should be noted that the developed interphase model given by Eqs. (33)–(36) are general in nature, and will replace the four governing equations for the traditional spring model given by (37) and (38). The new layer model can be used to deal with general boundary and loading conditions when the layer is bonded to different inner and outer media.

3. Results and discussion

In this section, the mechanical behavior of cylindrically layered media, shown in Fig. 1, is considered. The attention will be focussed on (i) the validation of the developed interphase model and (ii) the usage of this interphase model for evaluating the stress distribution in the layered media under different loading and geometric conditions.

3.1. Static axisymmetric problems

To evaluate the accuracy of the developed interphase model, consider first the stress field of an unbounded three-layer medium subjected to static axisymmetric loading $\sigma_r = p$, $\sigma_{r\theta} = 0$ at infinity. The middle layer is assumed to be isotropic so the closed form solution can be obtained. In this case, the general solution of the displacement field is,

Inner core

$$u_r = a_0 r \tag{39}$$

Middle layer

$$u_r = a_1 r + \frac{b_1}{r} \tag{40}$$

Outer medium

$$u_r = a_2 r + \frac{b_2}{r} \tag{41}$$

By applying the boundary conditions, $\sigma_r = p$, $\sigma_{r\theta} = 0$ at infinity, and the continuity conditions at the interfaces, the unknown constants in the general solution, a_0, a_1, a_2 and b_0, b_1, b_2, can be determined and the closed form solution of the problem can be obtained.

For this simple problem the solution based on the current interphase model can be obtained analytically. For the special case where the inner core is rigid and the Poisson's ratio is zero, the interphase model can be rewritten as,

$$\left(\frac{r_1\sigma^+_r-r_0\sigma^-_r}{r_1-r_0}\right)-E_1\left(\frac{u^+_r}{r_1+r_0}\right)=0 \tag{42}$$

$$\frac{1}{2}\left(\sigma^+_r+\sigma^-_r\right)-E_1\left(\frac{u^+_r}{r_1-r_0}\right)=0 \tag{43}$$

where '+' and '−' represent the corresponding values of the outer medium and the inner core at the two interfaces of the layer, with $u^-_r = 0$. $E_1 = c^{\langle 1\rangle}_{33}$ is the Young's modulus of the layer. Using the solution given by (39) and (41) and the boundary conditions at infinity, the stress field based on the current interphase model can be determined. The solution based on the interface-spring model, (37) and (38), can be similarly obtained.

The radial stress σ_r at the interface between the inner core and the layer ($r = r_0$) is

The exact solution:

$$\frac{\sigma_r^-}{p} = \frac{4}{2 + (\lambda_{21} - 1)(1 - \alpha^2)} \tag{44}$$

The current model:

$$\frac{\sigma_r^-}{p} = \frac{4 - \left(2(1-\alpha)^2/(\alpha+1)\right)}{2 + 2(\alpha - 1) + (1 - \alpha^2)\lambda_{21} + \left((1-\alpha)^2/(\alpha+1)\right)} \tag{45}$$

The spring model:

$$\frac{\sigma_r^-}{p} = \frac{4}{2 + 2\lambda_{21}(1 - \alpha)} \tag{46}$$

where $\alpha = r_0/r_1$, $\lambda_{21} = \frac{c_{33}^{(2)}}{c_{33}^{(1)}} = \frac{E_2}{E_1}$ with E_1 and E_2 being the Young's moduli of the layer and the outer medium, respectively.

Fig. 2 shows the comparison between the results of σ_r^-, given by (44)–(46), from the closed form solution, the current model, and the interface spring model for different E_2/E_1 ratios and layer thicknesses. For all three E_2/E_1 values considered, 0.5, 1.0 and 2.0, the current model shows an excellent agreement with the closed form solution even when the thickness of the layer is quite significant ($r_1/r_0 = 1.5$). The results are, however, very different from that by the interface spring model.

The extreme case where the core is a void is also considered for the validation of the model. In this case, $\sigma_r = 0$ at $r = r_0$ and the governing equations of the interphase model for the layer, (33)–(36), are reduced to

$$\frac{1}{2}(\sigma_r^+) - E_1\left(\frac{u_r^+ - u_r^-}{r_1 - r_0}\right) = 0 \tag{47}$$

$$\left(\frac{r_1\sigma_r^+}{r_1 - r_0}\right) - E_1\left(\frac{u_r^+ + u_r^-}{r_1 + r_0}\right) = 0 \tag{48}$$

with the hoop stress in the layer being given by

$$\sigma_\theta = E_1\left(\frac{u_r}{r}\right) = E_1\left(\frac{u_r^+ + u_r^-}{r_0 + r_1}\right) \tag{49}$$

By solving this problem, the hoop stress at $r = r_0^+$ in the layer is determined to be

The exact solution:

$$\frac{\sigma_\theta^-}{p} = \frac{4}{\lambda_{21}(1 + \alpha^2) + (1 - \alpha^2)} \tag{50}$$

The current model:

$$\frac{\sigma_\theta^-}{p} = \frac{4}{\lambda_{21}(3 + \alpha^2)/2 + 2(1 - \alpha)} \tag{51}$$

The spring model:

$$\frac{\sigma_\theta^-}{p} = 0. \tag{52}$$

The hoop stress at $r = r_1^+$ in the outer medium is

The exact solution:

$$\frac{\sigma_\theta^+}{p} = \frac{2}{1 + (1 - \alpha^2)/\lambda_{21}/(1 + \alpha^2)} \tag{53}$$

The current model:

$$\frac{\sigma_\theta^+}{p} = \frac{2}{1 + 4(1 - \alpha)/\lambda_{21}/(3 + \alpha^2)} \tag{54}$$

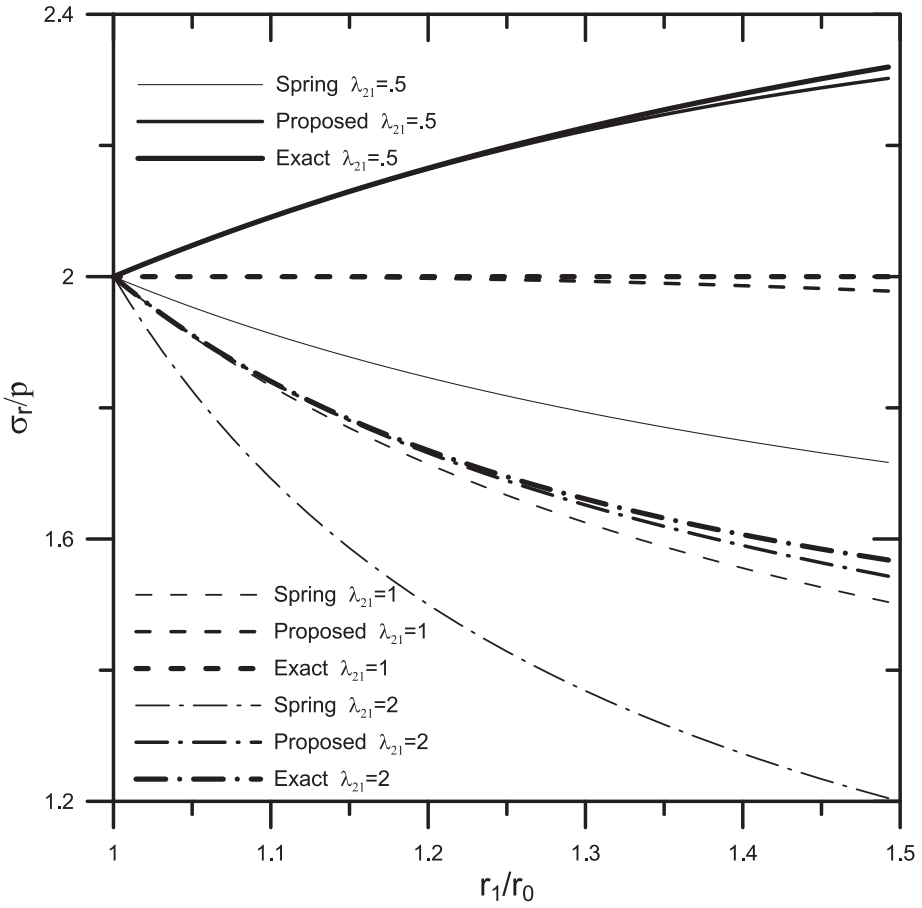

Fig. 2. Axisymmetric radial stress with a rigid core.

The spring model:

$$\frac{\sigma_\theta^+}{p} = 2. \tag{55}$$

Figs. 3 and 4 show the results of σ_θ^- and σ_θ^+, respectively, obtained from the closed form solution, the current model and the spring model, for different material combinations and geometries. For σ_θ^- shown in Fig. 3, the difference between the exact solution and the current model is within 10% even when the thickness of the layer reaches 30% of the radius of the inner core. The interface spring model, which predicts zero stress, is incapable of reasonably predicting the stress distribution. As shown in Fig. 4, σ_θ^+ from the current model coincides with that from the closed form solution, while the spring model predicts a constant stress $\sigma_\theta^+ = 2p$, which is quite different from the result of the closed form solution.

3.2. Bounded layered media subjected to surface loads

The current interphase model is used to simulate the dynamic behavior of a three-layer medium, shown in Fig. 1, under different loading conditions. Both the case shown in Fig. 1(a), which has an outer layer with a limited radius, and the case shown in Fig. 1(b), in which the radius of the outer layer is infinite, are considered to validate the interphase model and to study the dynamic response of the layered medium.

The difficulties in the analysis of such transversely anisotropic multilayered media are two folds. Firstly, the piezoelectric layer needs to be properly modeled to provide simple yet accurate description of the stress distribution in the layer. This is considered through the proposed interphase model. Secondly, in the numerical simulation the Bessel functions used need to be properly normalized (Ricks and Schmidt, 1994) to avoid overflow, which results in ill-conditioned (Zhang et al., 2010) equations. In the current simulation a numerical normalization algorithm is used to overcome this problem.

Material properties used in the study are shown in Table 1 (Qian et al., 2008; Nakatani et al., 2007). Different selections of material properties are considered in the simulation to study the effect of material combinations.

To evaluate the developed interphase model, consider the response of a finite three-layer medium shown in Fig. 5, subjected to a distributed surface load along the outer boundary $r = r_2$,

$$\sigma_r = \begin{cases} p & |\pi - \beta| \leqslant \theta \leqslant |\beta| \\ 0 & \text{elsewhere} \end{cases} \tag{56}$$

$$\sigma_{r\theta} = 0 \tag{57}$$

The applied surface stress can be expressed in terms of Fourier expansion as

$$\sigma_r = p\left(d_0 + \sum_{n=1}^{\infty} d_n \cos n\theta\right) \tag{58}$$

where

$$d_0 = \frac{2\beta}{\pi}, \quad d_n = \frac{2\sin(n\beta)}{\pi n}\left[1 + (-1)^n\right] \tag{59}$$

with p being the amplitude of the applied load and β being the range of the load.

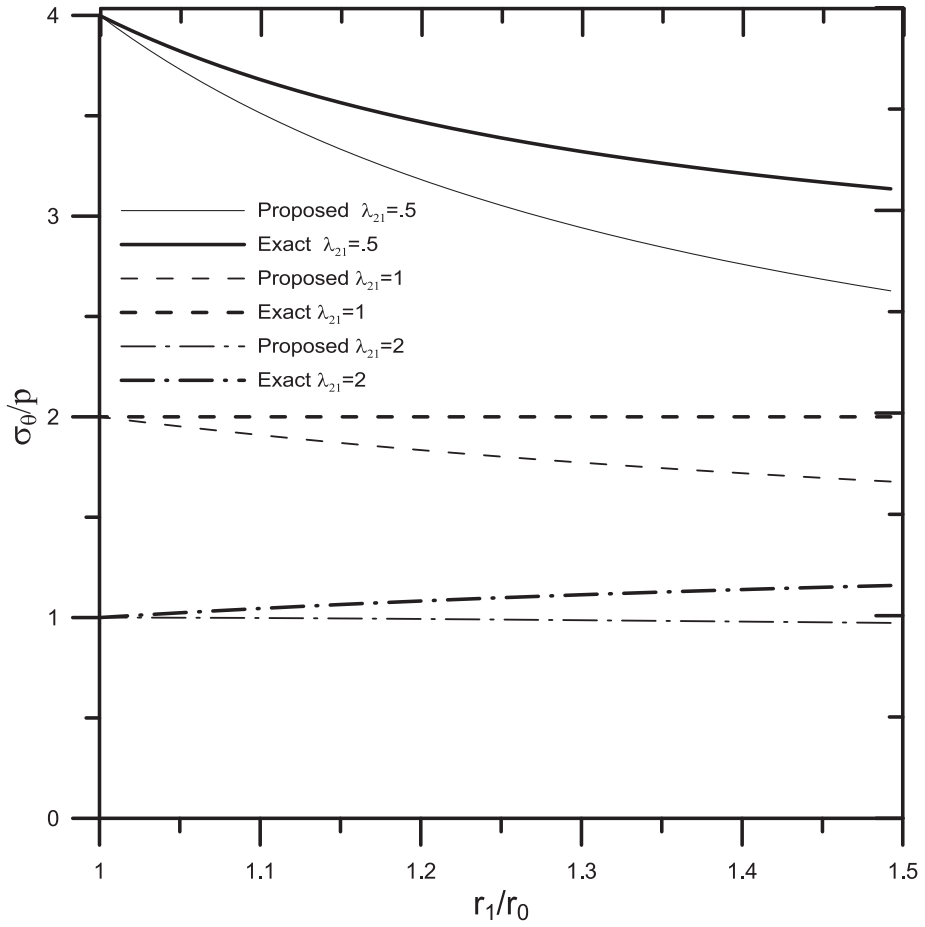

Fig. 3. Axisymmetric hoop stress with a void core: inner interface.

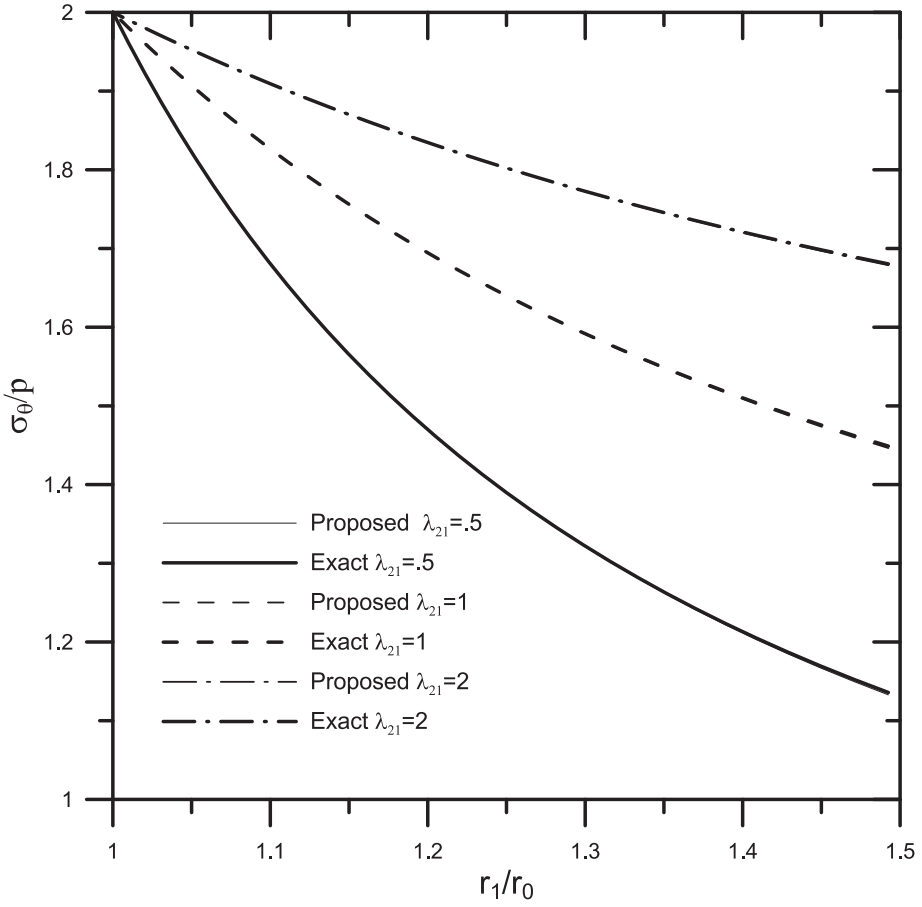

Fig. 4. Axisymmetric hoop stress with a void core: outer interface.

Table 1
Material constants used.

Material isotropic	Elastic constants $\times 10^{10}$ (N/m^2)					Density $\times 10^3$ (kg/m^2)	Piezoelectric $\times 10^0$ (C/m^2)	
	c_{22}	c_{33}	c_{12}	c_{23}	c_{44}	ρ	e_{31}	e_{33}
	c_{22}=c_{33}=$\lambda+2\mu$		λ	λ	μ			
Aluminum	11.27	11.27	6.07	6.07	2.6	2.7	–	–
Polythene	.554	.554	.298	.298	.128	1.2	–	–
PZT-4	13.9	12.4	6.78	7.43	2.5	7.5	−5.2	15.1
Steel	26.3	26.3	10.2	10.2	8.05	7.8	–	–

Fig. 6 shows the normalized radial stress distribution along the radial direction at $\theta = 0$ for the case where $\beta = \pi/6$ at a very low loading frequency $kR = 0.025$ with k being the shear wave number of the outer medium $k_T = \omega/c_T$, R being the outer radius of the interphase, $R = r_1$, and $r_2 = 1.5r_1$. To evaluate the accuracy of the current interphase model, the core, the interphase and the outer layer are assumed to be of the same material and different interphase thicknesses are considered. The results from the interface-spring model, the current model and the finite element analysis (ANSYS) are compared. For layer thicknesses $h/R = 0.1, 0.2, 0.3$ the current model shows a very good agreement with the finite element results, while the interface-spring model shows much more significant errors for all thicknesses considered. The corresponding distribution of σ_θ along $\theta = 0$ is given in Fig. 7. Again the current model provides excellent prediction of the stress distribution but the result from the interface-spring model is quite different from the finite element prediction around the middle layer. The corresponding dynamic stress σ_r is shown in Figs. 8 and 9 for $kR = 0.5$ and $kR = 1.1$ for different layer thicknesses. The simulation results indicate that for very small thickness $h/R = 0.01$ the interface-spring model, the current model and the finite element analysis provide almost identical results. But for larger thicknesses of the layer $(h/R = 0.1, 0.2, 0.3)$, the current model shows much better results in comparison with the interface-spring model.

Figs. 10 and 11 show the corresponding radial stress distribution for dissimilar media at $kR = 0.4$ and 0.8, respectively, with the outer layer being aluminum, the core being steel and the middle layer being PZT-4. For very thin layer, $h/R = 0.01$, the results from the FEM, the current model and the interface spring model are almost identical. But for $h/R = 0.1, 0.2, 0.3$, the spring model shows significant different results from the current model and the FEM.

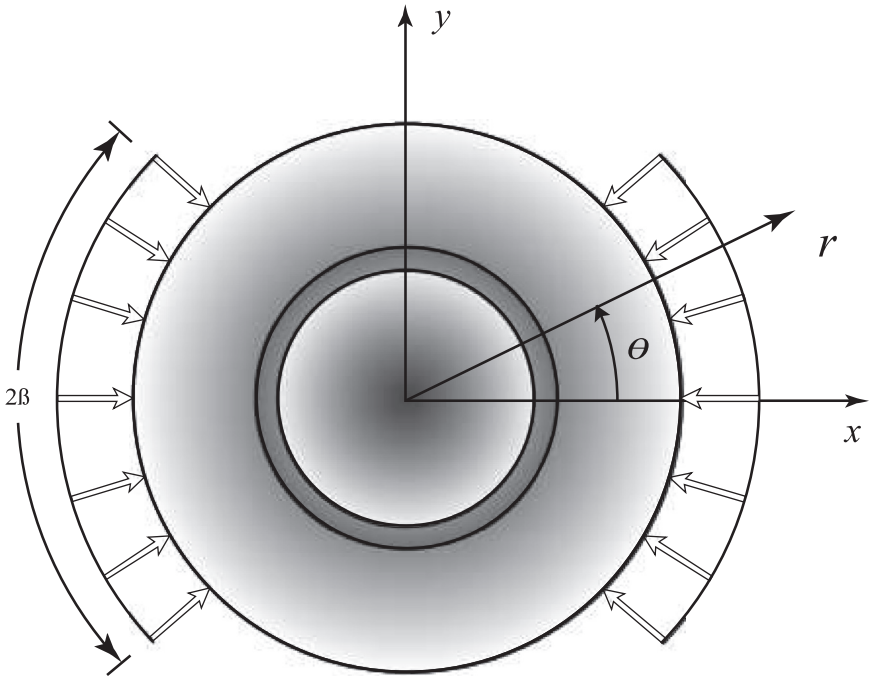

Fig. 5. Bounded layered medium subjected to surface loads.

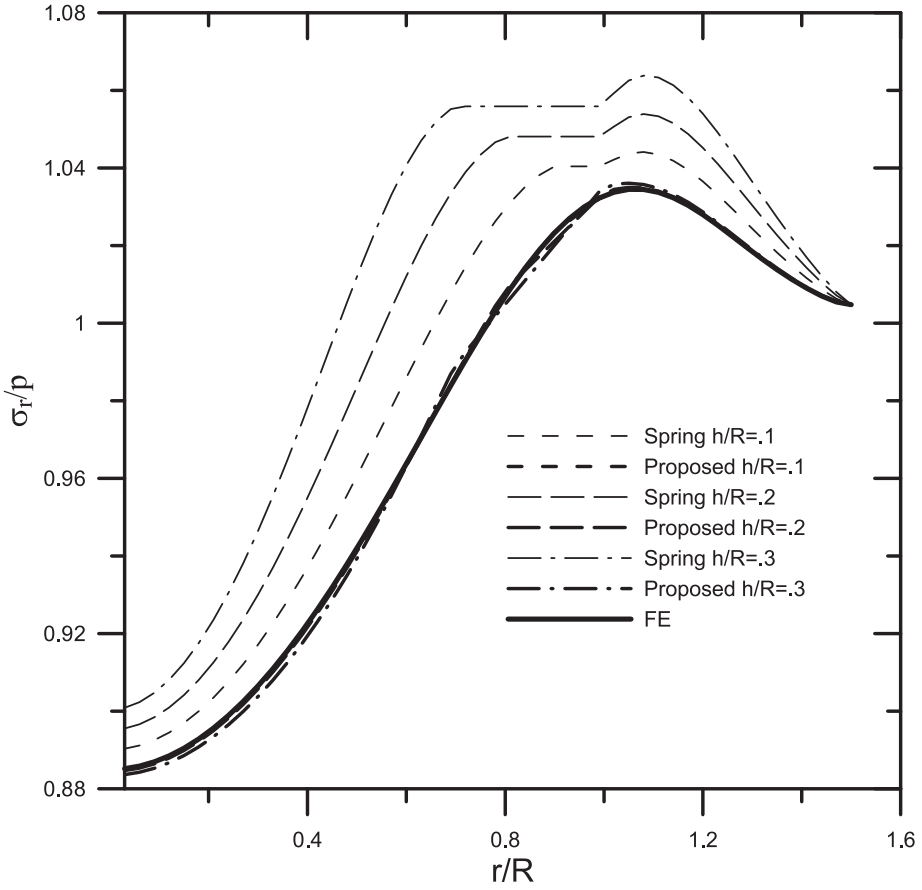

Fig. 6. Radial stress distribution for a homogenous medium at $kR = 0.025$.

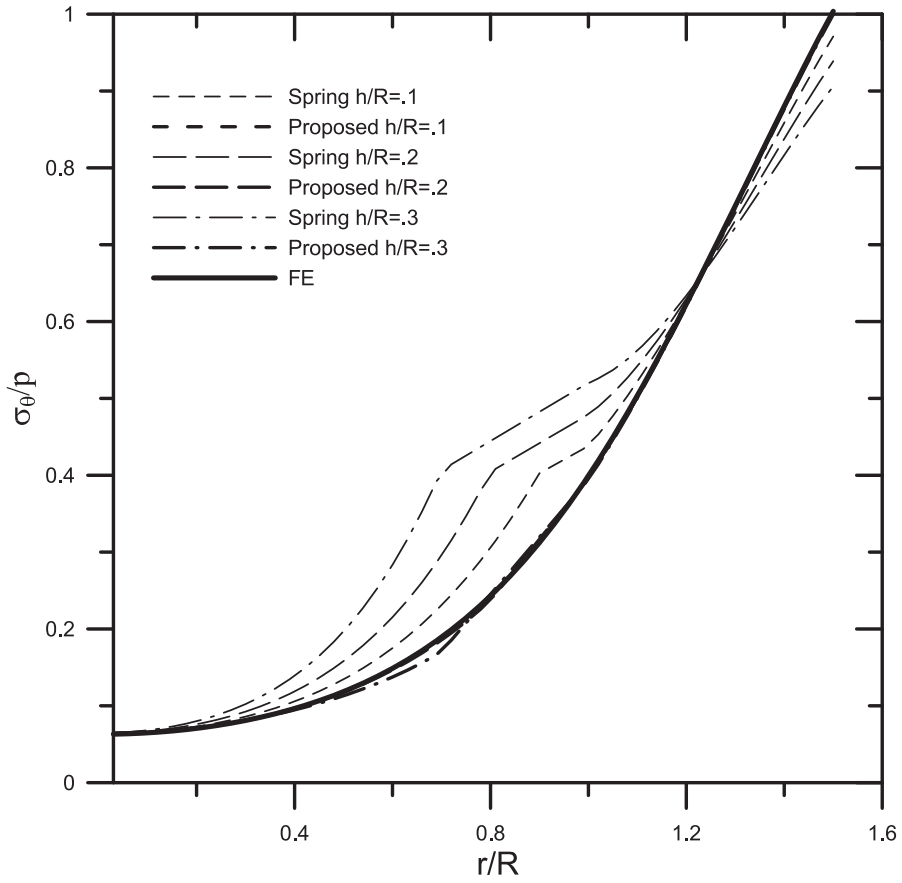

Fig. 7. Hoop stress distribution for a homogenous medium at $kR = 0.025$.

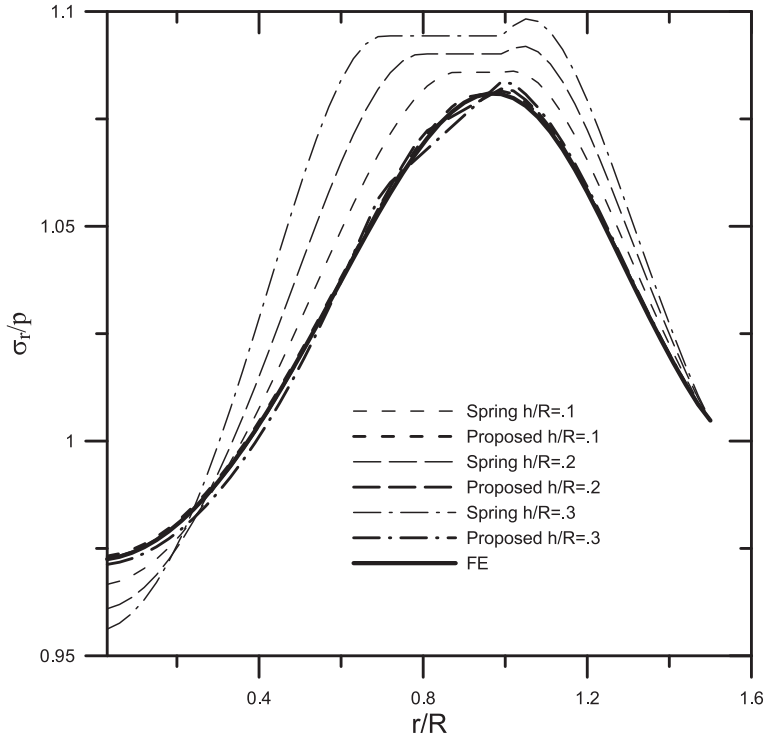

Fig. 8. Radial stress distribution for a homogenous medium at $kR = 0.5$.

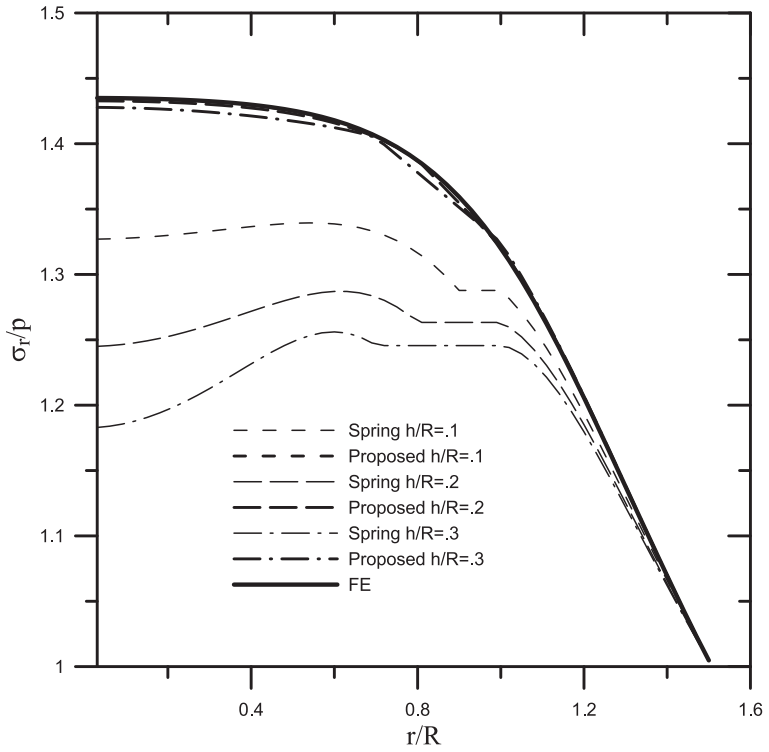

Fig. 9. Radial stress distribution for a homogenous medium at $kR = 1.1$.

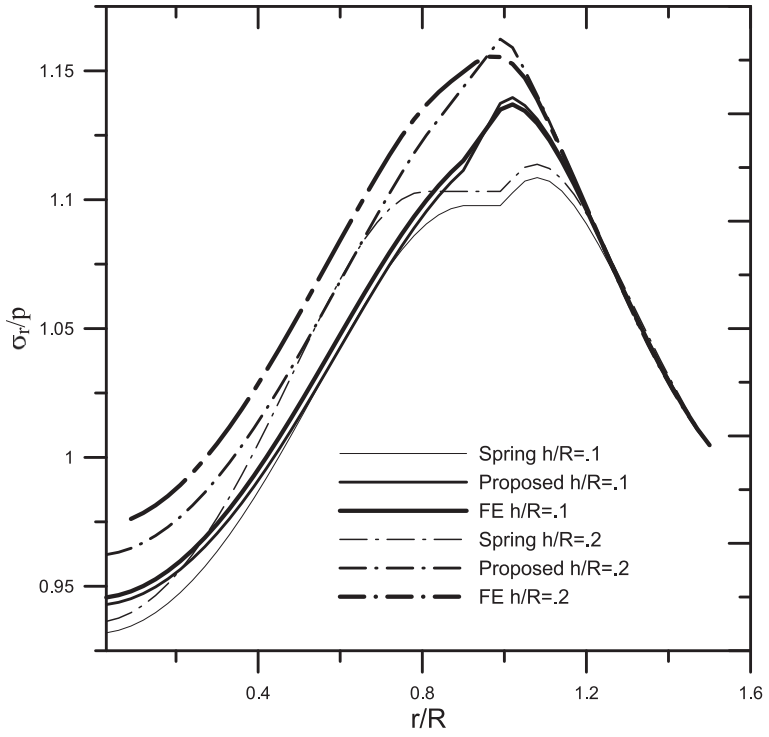

Fig. 10. Radial stress distribution for a dissimilar medium at $kR = 0.4$.

3.3. Infinite layered media subjected to incident waves

Consider now the dynamic response of a layered medium with an infinite outer medium ($r_2 = \infty$) subjected to an incident P-wave, as shown in Fig. 1(b). The incident P-wave with a general incident angle θ_0 can be expressed in terms of the displacement potential as

$$\varphi^{in} = \varphi_0 e^{-ik_L r\cos(\theta-\theta_0)} \tag{60}$$

where φ_0 is the magnitude of the incident wave, and k_L is the longitudinal wave number of the outer medium. In the following discussion, $\theta_0 = 0$ is considered. The incident displacement and stress fields can be determined from φ^{in} directly.

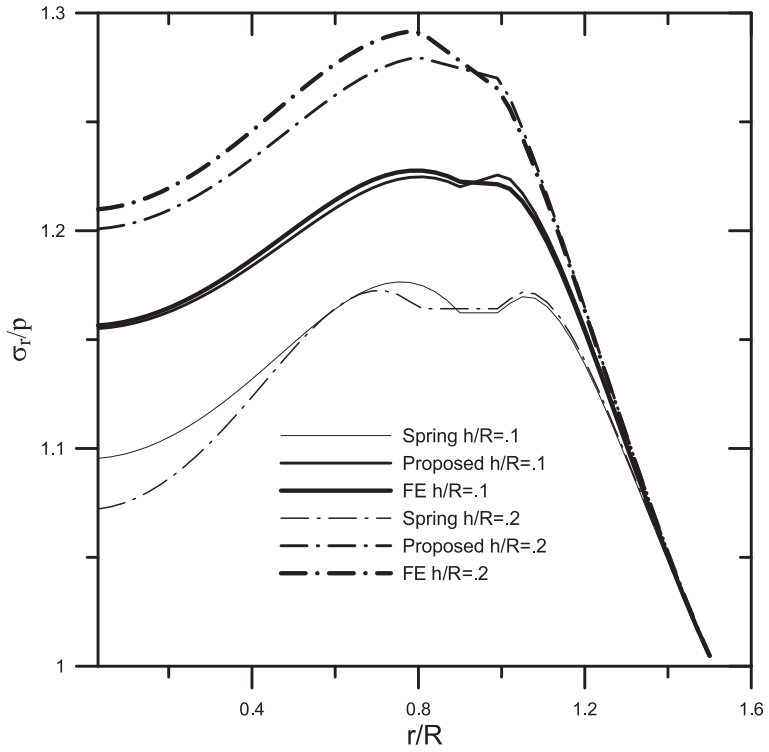

Fig. 11. Radial stress distribution for a dissimilar medium at $kR = 0.8$.

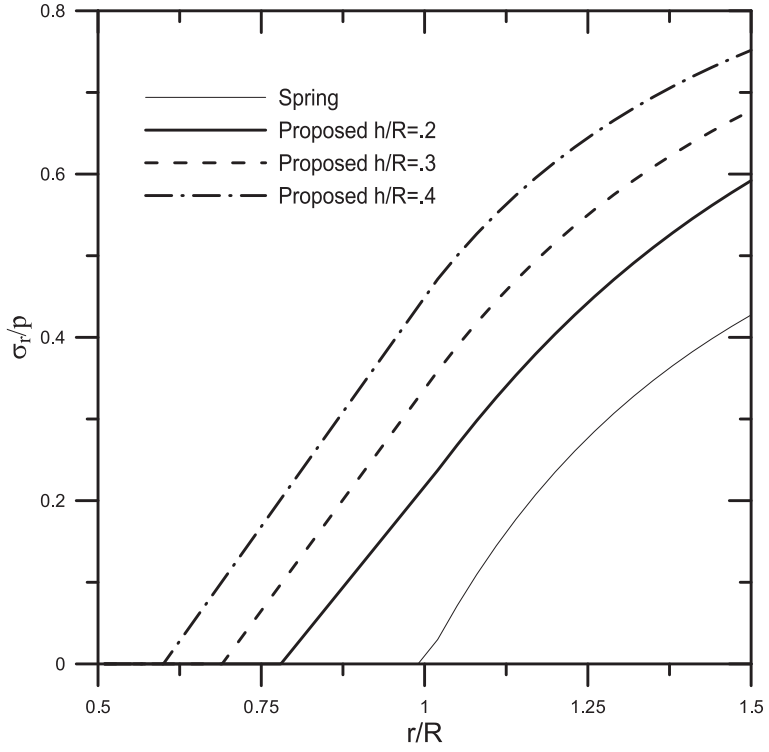

Fig. 12. Radial stress distribution for a dissimilar medium with a void core at $kR = 0.01$.

The total field in the outer medium consists of an incident field and a scattered field. By separating the incident field from the total field, the governing equations of the current interphase model become

$$\frac{1}{r^2}\left\{\frac{r_1^2\sigma_{r\theta}^{sc}-r_0^2\sigma_{r\theta}^{-}}{h}+r\left[c_{23}\frac{u_{r,\theta}^{sc}-u_{r,\theta}^{-}}{h}+\frac{c_{22}}{r}\left(-n^2\frac{u_{\theta}^{sc}+u_{\theta}^{-}}{2}+\frac{u_{r,\theta}^{sc}+u_{r,\theta}^{-}}{2}\right)\right]\right\} = \sigma_{r\theta}^{*}-\rho\omega^2 u_{\theta} \tag{61}$$

$$\frac{1}{r}\left\{\frac{r_1\sigma_r^{sc}-r_0\sigma_r^-}{h}+\frac{\sigma_{r\theta,\theta}^{sc}+\sigma_{r\theta,\theta}^-}{2}-\left[c_{23}\frac{u_r^{sc}-u_r^-}{h}+\frac{c_{22}}{r}\left(\frac{u_{\theta,\theta}^{sc}+u_{\theta,\theta}^-}{2}+\frac{u_r^{sc}+u_r^-}{2}\right)\right]\right\} = \sigma_r^*-\rho\omega^2 u_r \tag{62}$$

$$\frac{\sigma_r^{sc}+\sigma_r^-}{2}-\left\{c_{33}\frac{u_r^{sc}-u_r^-}{h}+\frac{c_{23}}{r}\left(\frac{u_{\theta,\theta}^{sc}+u_{\theta,\theta}^-}{2}+\frac{u_r^{sc}+u_r^-}{2}\right)\right\} = u_r^* \tag{63}$$

$$\frac{\sigma_{r\theta}^{sc}+\sigma_{r\theta}^-}{2}-c_{44}\left(\frac{1}{r}\frac{u_{r,\theta}^{sc}+u_{r,\theta}^-}{2}+\frac{u_\theta^{sc}-u_\theta^-}{h}-\frac{1}{r}\frac{u_\theta^{sc}+u_\theta^-}{2}\right) = u_\theta^* \tag{64}$$

where the superscript 'sc' represents the scattered field in the outer medium to be determined from the solution, and the terms with superscript '$*$' represent the incident wave, which are given by

$$u_r^* = -\frac{\sigma_r^{in}}{2}+c_{33}\frac{u_r^{in}}{h}+\frac{c_{23}}{r}\left[\frac{\partial}{\partial\theta}\left(\frac{u_\theta^{in}}{2}\right)+\frac{u_r^{in}}{2}\right] \tag{65}$$

$$\sigma_r^* = -\frac{1}{r}\left\{\frac{r_1\sigma_r^{in}}{h}+\frac{\sigma_{r\theta,\theta}^{in}}{2}-\left[c_{23}\frac{u_r^{in}}{h}+\frac{c_{22}}{r}\left(\frac{u_{\theta,\theta}^{in}}{2}+\frac{u_r^{in}}{2}\right)\right]\right\} \tag{66}$$

$$u_\theta^* = -\frac{\sigma_{r\theta}^{in}}{2}+c_{44}\left[\frac{u_{r,\theta}^{in}}{2r}+\frac{u_\theta^{in}}{h}-\frac{u_\theta^{in}}{2r}\right] \tag{67}$$

$$\sigma_{r\theta}^* = -\frac{1}{r^2}\left\{\frac{r_1^2\sigma_{r\theta}^{in}}{h}+r\left[c_{23}\frac{u_{r,\theta}^{in}}{h}+\frac{c_{22}}{r}\left(-n^2\frac{u_\theta^{in}}{2}+\frac{u_{r,\theta}^{in}}{2}\right)\right]\right\}. \tag{68}$$

Fig. 12 shows the normalized radial stress distribution along $\theta = 0$ caused by an incident wave with a very low loading frequency $kR = 0.01$ with p being the magnitude of the maximum stress of the incident wave. In this case the inner core is void, the middle layer is PZT-4 and the outer medium is aluminum. For different PZT layer thicknesses, the radial stress shows a monotonic increase from the inner surface of the PZT layer. The result from the spring model, however, could not capture the variation of the stress in the layer. Similar results are observed for the corresponding problem with a higher loading frequency, $kR = 0.6$, as shown in Fig. 13.

Fig. 14 shows the corresponding radial stress distribution for the case where the inner core is steel, the middle layer is PZT-4 and the outer medium is polythene, subjected to an incident wave of low frequency $kR = 0.01$. Both the current model and the spring model could predict the well-known result that the stress in the core is a constant for such a static load. But the spring model is not sensitive to the change of the thickness of the middle layer, which has been reasonably predicted by the current interphase model. Figs. 15 and 16 show the corresponding normalized radial stress distribution along $\theta = 0$ with $kR = 0.02$ and $kR = 0.9$, for the case where the inner core is steel, the middle layer is PZT-4 and the outer medium is aluminum. For different PZT layer thicknesses considered, which are rather large, the result from the spring model shows significant difference from that by the current model.

4. Conclusions

The proposed interphase model for cylindrical anisotropic layers, which contains the effect of the hoop stress and satisfies the equations of motion, shows an excellent accuracy in simulating the stress distribution, and agrees well with the FEM prediction. The proposed model is significantly superior to the traditional interface spring model and, as a result, provides an efficient way to model complicated dynamic deformation caused by anisotropic layers. The current model has been verified at frequencies lower or higher than typical resonance frequencies. It has also been used in situations where the thickness of the layer is significant large, 30% of the typical radius for example. The model can be used to accurately simulate dynamic behavior of cylindrical anisotropic layers, which are otherwise difficult to dealt with.

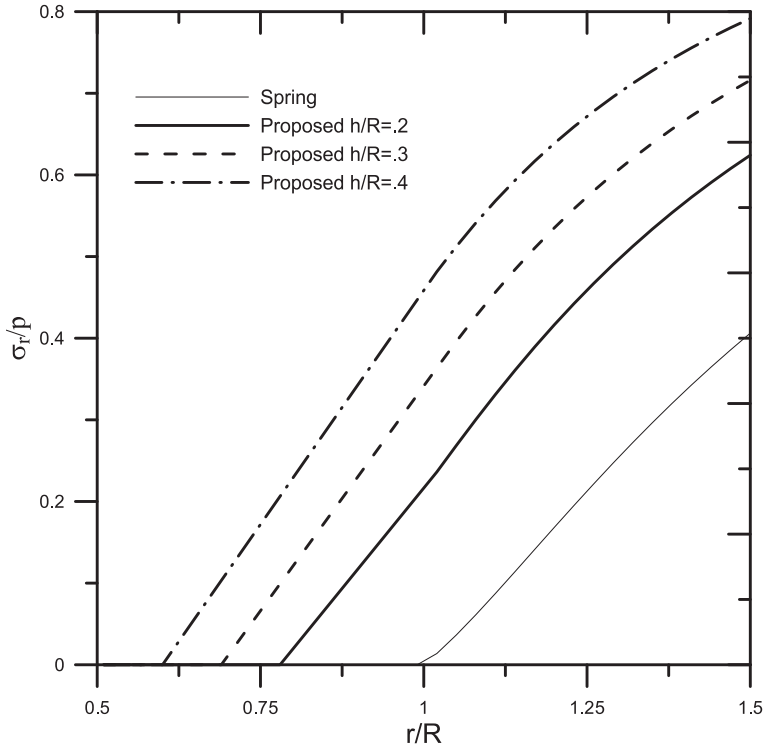

Fig. 13. Radial stress distribution for a dissimilar medium with a void core at $kR = 0.6$.

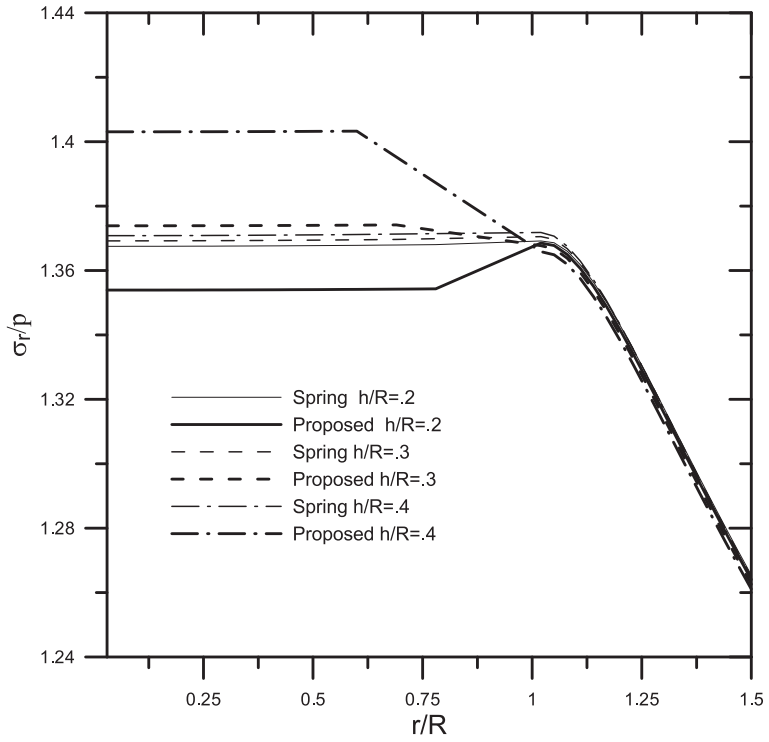

Fig. 14. Radial stress distribution for a dissimilar medium with a stiff core at $kR = 0.01$.

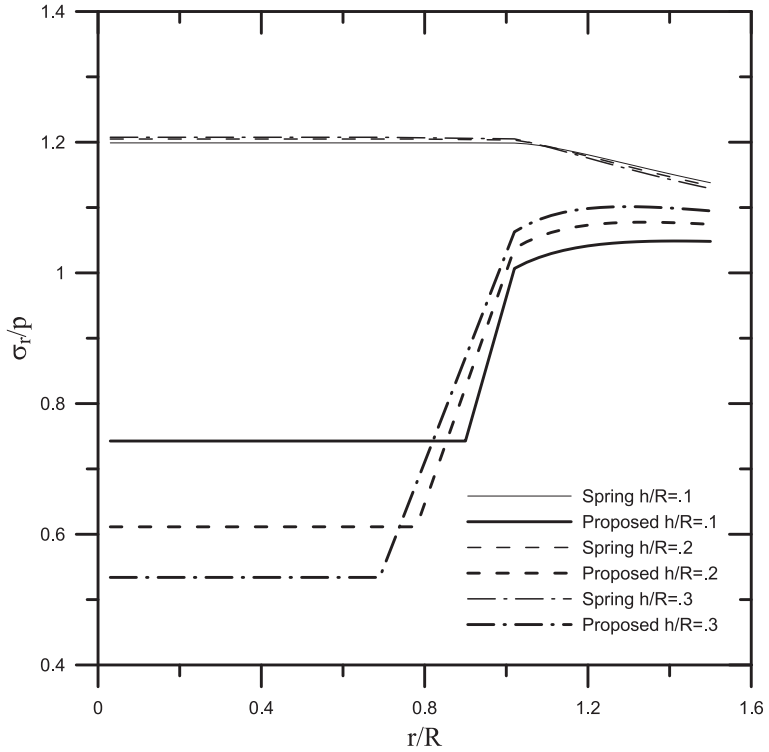

Fig. 15. Radial stress distribution for a dissimilar medium at $kR = 0.02$.

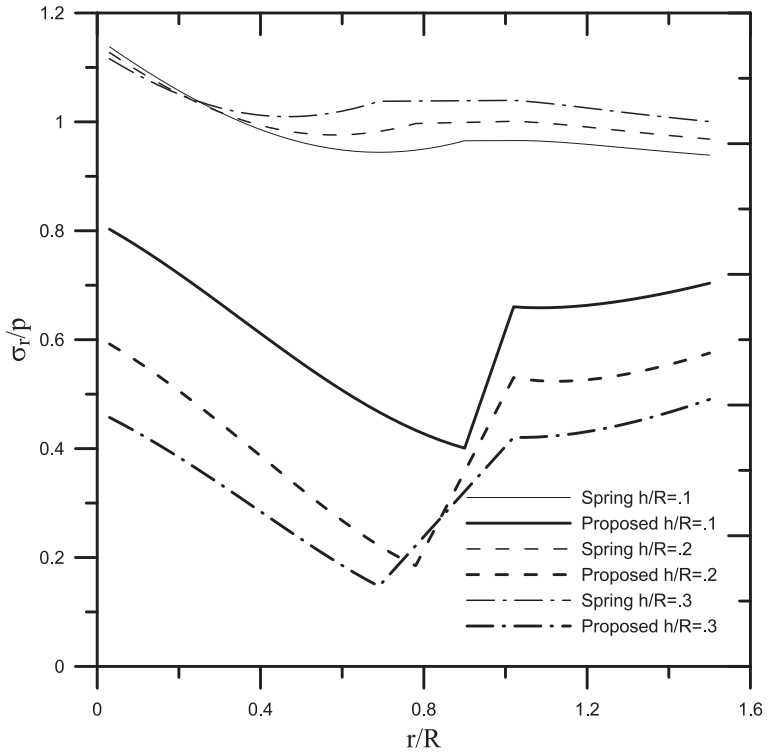

Fig. 16. Radial stress distribution for a dissimilar medium at $kR = 0.9$.

Acknowledgment

This research was supported by the Natural Sciences and Engineering Research Council of Canada (NSERC).

Appendix A

The general elastic solution of an isotropic layer can be obtained using displacement potentials. The results are presented in this section. The displacements can be expressed in terms of the displacement potentials as:

$$u_r = \varphi_{,r} + \frac{1}{r}\psi_{,\theta}, u_\theta = \frac{1}{r}\varphi_{,\theta} - \psi_{,r}.$$

The stress components are

$$\sigma_r = \lambda\nabla^2\varphi + 2\mu\left[\varphi_{,r^2} + \left(\frac{1}{r}\psi_{,\theta}\right)_{,r}\right]$$

$$\sigma_\theta = \lambda\nabla^2\varphi + 2\mu\left[\frac{1}{r}\left(\varphi_{,r} + \frac{1}{r}\varphi_{,\theta^2}\right) + \frac{1}{r}\left(\frac{1}{r}\psi_{,\theta} - \psi_{,r\theta}\right)\right]$$

$$\sigma_{r\theta} = \mu\left[2\left(\frac{1}{r}\varphi_{,r\theta} - \frac{1}{r^2}\varphi_{,\theta}\right) + \left(\frac{1}{r^2}\psi_{,\theta^2} - r\left(\frac{1}{r}\psi_{,r}\right)_r\right)\right].$$

Using the general solution of the displacement potentials given by Eqs. (17) and (18). The displacement and stress fields can be obtained as

$$u_r = \sum_{n=0}^{\infty} k_L\left\{J_n'(k_Lr)\begin{pmatrix}A_n^{(1)}\\A_n^{(2)}\end{pmatrix}^T + H_n'(k_Lr)\begin{pmatrix}A_n^{(3)}\\A_n^{(4)}\end{pmatrix}^T\right\}\begin{pmatrix}cos(n\theta)\\sin(n\theta)\end{pmatrix} + \frac{n}{r}\left\{J_n(k_sr)\begin{pmatrix}-A_n^{(5)}\\A_n^{(6)}\end{pmatrix}^T + H_n(k_sr)\begin{pmatrix}-A_n^{(7)}\\A_n^{(8)}\end{pmatrix}^T\right\}\begin{pmatrix}sin(n\theta)\\cos(n\theta)\end{pmatrix}$$

$$u_\theta = \sum_{n=0}^{\infty}\frac{n}{r}\left\{J_n(k_Lr)\begin{pmatrix}-A_n^{(1)}\\A_n^{(2)}\end{pmatrix}^T + H_n(k_Lr)\begin{pmatrix}-A_n^{(3)}\\A_n^{(4)}\end{pmatrix}^T\right\}\begin{pmatrix}sin(n\theta)\\cos(n\theta)\end{pmatrix} - k\left\{J_n'(k_sr)\begin{pmatrix}A_n^{(5)}\\A_n^{(6)}\end{pmatrix}^T + H_n'(k_sr)\begin{pmatrix}A_n^{(7)}\\A_n^{(8)}\end{pmatrix}^T\right\}\begin{pmatrix}cos(n\theta)\\sin(n\theta)\end{pmatrix}$$

$$\sigma_r = \sum_{n=0}^{\infty}\left(J_n'(k_Lr)k_L\frac{\lambda}{r} + J_n''(k_Lr)k_L^2(\lambda+2\mu) - J_n(k_Lr)n^2\frac{\lambda}{r^2}\right)\begin{pmatrix}A_n^{(1)}\\A_n^{(2)}\end{pmatrix}^T\begin{pmatrix}cos(n\theta)\\sin(n\theta)\end{pmatrix} + \sum_{n=0}^{\infty}\left(H_n'(k_Lr)k_L\frac{\lambda}{r} + H_n''(k_Lr)k_L^2(\lambda+2\mu) - H_n(k_Lr)n^2\frac{\lambda}{r^2}\right)\begin{pmatrix}A_n^{(3)}\\A_n^{(4)}\end{pmatrix}^T \times\begin{pmatrix}cos(n\theta)\\sin(n\theta)\end{pmatrix} + \sum_{n=0}^{\infty}\left(\frac{J_n(k_sr)}{r} - J_n'(k_sr)k_s\right)\frac{2\mu n}{r}\begin{pmatrix}A_n^{(5)}\\-A_n^{(6)}\end{pmatrix}^T\begin{pmatrix}sin(n\theta)\\cos(n\theta)\end{pmatrix} + \sum_{n=0}^{\infty}\left(\frac{H_n(k_sr)}{r} - H_n'(k_sr)k_s\right)\frac{2\mu n}{r}\begin{pmatrix}A_n^{(7)}\\-A_n^{(8)}\end{pmatrix}^T\begin{pmatrix}sin(n\theta)\\cos(n\theta)\end{pmatrix}$$

$$\sigma_{r\theta} = \mu\left\{\sum_{n=0}^{\infty}\left(\frac{J_n(k_Lr)}{r} - J_n'(k_Lr)k_L\right)\frac{2n}{r}\begin{pmatrix}A_n^{(1)}\\-A_n^{(2)}\end{pmatrix}^T\begin{pmatrix}sin(n\theta)\\cos(n\theta)\end{pmatrix} + \sum_{n=0}^{\infty}\left(\frac{H_n(k_Lr)}{r} - H_n'(k_Lr)k_L\right)\frac{2n}{r}\begin{pmatrix}A_n^{(3)}\\-A_n^{(4)}\end{pmatrix}^T\begin{pmatrix}sin(n\theta)\\cos(n\theta)\end{pmatrix} + \sum_{n=0}^{\infty}\left(-J_n''(k_sr)k_s^2 - J(k_sr)\frac{n^2}{r^2} + J_n'(k_sr)\frac{k_s}{r}\right)\begin{pmatrix}A_n^{(5)}\\A_n^{(6)}\end{pmatrix}^T\begin{pmatrix}cos(n\theta)\\sin(n\theta)\end{pmatrix} + \sum_{n=0}^{\infty}\left(-H_n''(k_sr)k_s^2 - H_n(k_sr)\frac{n^2}{r^2} + H_n'(k_sr)\frac{k_s}{r}\right)\begin{pmatrix}A_n^{(7)}\\A_n^{(8)}\end{pmatrix}^T\begin{pmatrix}cos(n\theta)\\sin(n\theta)\end{pmatrix}\right\}$$

$$\sigma_\theta = \sum_{n=0}^{\infty}\left(J_n''(k_Lr)k_L^2\lambda - J_n(k_Lr)(\lambda+2\mu)\frac{n^2}{r^2} + \frac{(\lambda+2\mu)}{r}J_n'(k_Lr)k_L\right) \times \begin{pmatrix} A_n^{(1)} \\ A_n^{(2)} \end{pmatrix}^T \begin{pmatrix} cos(n\theta) \\ sin(n\theta) \end{pmatrix} + \sum_{n=0}^{\infty}\left(\lambda H_n''(k_Lr)k_L^2 - H_n(k_Lr)(\lambda+2\mu)\frac{n^2}{r^2} + H_n'(k_Lr)k_L\frac{(\lambda+2\mu)}{r}\right) \times \begin{pmatrix} A_n^{(3)} \\ A_n^{(4)} \end{pmatrix}^T \begin{pmatrix} cos(n\theta) \\ sin(n\theta) \end{pmatrix} + \sum_{n=0}^{\infty}\left(\frac{J_n(k_sr)}{r} - J_n'(k_sr)k_s\right)\frac{2\mu n}{r}\begin{pmatrix} -A_n^{(5)} \\ A_n^{(6)} \end{pmatrix}^T \begin{pmatrix} sin(n\theta) \\ cos(n\theta) \end{pmatrix} + \sum_{n=0}^{\infty}\left(\frac{H_n(k_sr)}{r} - H_n'(k_sr)k_s\right)\frac{2\mu n}{r}\begin{pmatrix} A_n^{(7)} \\ -A_n^{(8)} \end{pmatrix}^T \begin{pmatrix} sin(n\theta) \\ cos(n\theta) \end{pmatrix}.$$

References

Aboudi, J., 1987. Damage in composites-modeling of imperfect bonding. Composites Science and Technology 28, 103–128.

Achenbach, J., 1972. Wave Propagation in Elastic Solids, vol. 39. North Holland.

Bian, Z., Chen, W., Lu, C., 2008. Wave propagation in two-layered infinite composite piezoelectric hollow cylinder with imperfect interfaces. In: Symposium on, IEEE Piezoelectricity, Acoustic Waves, and Device Applications, SPAWDA 2008, pp. 315–319.

Egusa, S., Wang, Z., Chocat, N., Ruff, Z., Stolyarov, A., Shemuly, D., Sorin, F., Rakich, P., Joannopoulos, J., Fink, Y., 2010. Multimaterial piezoelectric fibers. Nature Materials 9, 643–648.

Gibson, R., 2010. A review of recent research on mechanics of multifunctional composite materials and structures. Composite Structures 92, 2793–2810.

Gsell, D., Dual, J., 2004. Non-destructive evaluation of elastic material properties in anisotropic circular cylindrical structures. Ultrasonics 43, 123–132.

Honarvar, F., Sinclair, A., 1996. Acoustic wave scattering from transversely isotropic cylinders. The Journal of the Acoustical Society of America 100, 57–63.

Kessler, D., Kosloff, D., 1991. Elastic wave propagation using cylindrical coordinates. Geophysics 56, 2080–2089.

Kreja, I., 2011. A literature review on computational models for laminated composite and sandwich panels. Central European Journal of Engineering, 1–22.

Kushch, V., Shmegera, S., Brndsted, P., Mishnaevsky Jr, L., 2011. Numerical simulation of progressive debonding in fiber reinforced composite under transverse loading. International Journal of Engineering Science 49, 17–29.

Librescu, L., Schmidt, R., 2001. A general linear theory of laminated composite shells featuring interlaminar bonding imperfections. International Journal of Solids and Structures 38, 3355–3375.

Lin, Y., Sodano, H., 2008. Concept and model of a piezoelectric structural fiber for multifunctional composites. Composites Science and Technology 68, 1911–1918.

Nakatani, K., Kubo, S., Sakagami, T., Shiozawa, D., Takagi, M., 2007. An experimental study on the identification of delamination in a composite material by the passive electric potential CT method. Measurement Science and Technology 18, 49–56.

Nayfeh, A., 1995. Wave Propagation in Layered Anisotropic Media: With Applications to Composites, vol. 39. North Holland.

Nayfeh, A., Nagy, P., 1996. General study of axisymmetric waves in layered anisotropic fibers and their composites. Journal of the Acoustical Society of America 99, 931–941.

Nayfeh, A., Abdelrahman, W., Nagy, P., 2000. Analyses of axisymmetric waves in layered piezoelectric rods and their composites. The Journal of the Acoustical Society of America 108, 1496–1504.

Norris, A., Shuvalov, A., 2010. Wave impedance matrices for cylindrically anisotropic radially inhomogeneous elastic solids. The Quarterly Journal of Mechanics and Applied Mathematics 63, 401–435.

Norris, A., Shuvalov, A., 2012. Elastodynamics of radially inhomogeneous spherically anisotropic elastic materials in the Stroh formalism. Proceedings of the Royal Society A: Mathematical, Physical and Engineering Science 468, 467–484.

Qian, Z., Jin, F., Kishimoto, K., Lu, T., 2008. Scattering of elastic p-waves by a transversely isotropic piezoelectric cylinder embedded in a polymer matrix. Smart Materials and Structures 17, 045019.

Rajabi, M., Hasheminejad, S., 2009. Acoustic resonance scattering from a multilayered cylindrical shell with imperfect bonding. Ultrasonics 49, 682–695.

Ricks, D., Schmidt, H., 1994. A numerically stable global matrix method for cylindrically layered shells excited by ring forces. The Journal of the Acoustical Society of America 95, 3339–3349.

Rokhlin, S., Huang, W., 1992. Ultrasonic wave interaction with a thin anisotropic layer between two anisotropic solids: exact and asymptotic-boundary-condition methods. The Journal of the Acoustical Society of America 92, 1729–1742.

Rokhlin, S., Huang, W., 1993. Ultrasonic wave interaction with a thin anisotropic layer between two anisotropic solids. II: Second-order asymptotic boundary conditions. The Journal of the Acoustical Society of America 94, 3405–3420.

Sodagar, S., Honarvar, F., 2010. Improvements to the mathematical model of acoustic wave scattering from transversely isotropic cylinders. Scientia Iranica Transaction B: Mechanical Engineering 17, 157–166.

Zhang, J., Li, T., Ye, W., Zhu, X., 2010. Acoustic radiation of damped cylindrical shell with arbitrary thickness in the fluid field. Journal of Marine Science and Application 9, 431–438.

Zhong, Z., Meguid, S., 1997. Interfacial debonding of a circular inhomogeneity in piezoelectric materials. International Journal of Solids and Structures 34, 1965–1984.